# How fiber bundle alterations differ in presumed LATE and amnestic Alzheimer's disease

Aurélie Lebrun, Yann Leprince, Julien Lagarde, Pauline Olivieri, Martin Moussion, Camille Noiray, Michel Bottlaender, Marie Sarazin

Received: 28 February 2024 | Revised: 29 May 2024 | Accepted: 9 July 2024

DOI: 10.1002/alz.14156

Alzheimer's & Dementia®
THE JOURNAL OF THE ALZHEIMER'S ASSOCIATION

RESEARCH ARTICLE

# How fiber bundle alterations differ in presumed LATE and amnestic Alzheimer's disease

**Aurélie Lebrun**[1,2] | **Yann Leprince**[1] | **Julien Lagarde**[2,3,4] | **Pauline Olivieri**[3] | **Martin Moussion**[3,5] | **Camille Noiray**[3,4] | **Michel Bottlaender**[1,2] | **Marie Sarazin**[2,3,4]

[1]Université Paris-Saclay, UNIACT, NeuroSpin, CEA, Gif-sur-Yvette, France

[2]Université Paris-Saclay, BioMaps, Service Hospitalier Frédéric Joliot, CEA, CNRS, Inserm, Orsay, France

[3]Department of Neurology of Memory and Language, GHU Paris Psychiatrie & Neurosciences, Hôpital Sainte-Anne, Paris, France

[4]Université Paris-Cité, Paris, France

[5]Centre d'Evaluation Troubles Psychiques et Vieillissement, GHU Paris Psychiatrie & Neurosciences, Hôpital Sainte Anne, Paris, France

**Correspondence**
Aurélie Lebrun and Yann Leprince, NeuroSpin, Centre d'études de Saclay, Bâtiment 145, Gif-sur-Yvette 91191, France.
Email: aurelie.lebrun@cea.fr and yann.leprince@cea.fr

**Funding information**
French Ministry of Health, Grant/Award Numbers: PHRC-2013-0919, PHRC- 0054-N 2010; CEA; Fondation pour la recherche sur la maladie d'Alzheimer; Institut de Recherches Internationales Servier; Fondation France-Alzheimer; Institut Roche de Recherche et Médecine Translationnelle

## Abstract

**INTRODUCTION:** Typical Alzheimer's disease (AD) and limbic-predominant age-related TAR DNA-binding protein 43 (TDP-43) encephalopathy (LATE) are two neurodegenerative diseases that present with a similar initial amnestic clinical phenotype but are associated with distinct proteinopathies.

**METHODS:** We investigated white matter (WM) fiber bundle alterations, using fixel-based analysis, a state-of-the-art diffusion magnetic resonance imaging model, in early AD, presumed LATE, and controls. We also investigated regional cortical atrophy.

**RESULTS:** Both amnestic AD and presumed LATE patients exhibited WM alterations in tracts of the temporal and limbic lobes and in callosal fibers connecting superior frontal gyri. In addition, presumed LATE patients showed alterations in callosal fibers connecting the middle frontal gyri and in the cerebello–thalamo–cortical tract. Cortical thickness was reduced in regions connected by the most altered tracts.

**DISCUSSION:** These findings, the first to describe WM fiber bundle alterations in presumed LATE, are consistent with results on cortical atrophy and with the staging system of tau or TDP-43 accumulation.

KEYWORDS
Alzheimer's disease, diffusion magnetic resonance imaging, fixel-based analysis, limbic-predominant age-related TAR DNA-binding protein 43 encephalopathy, white matter

## Highlights

- Fixel-based analysis revealed white matter (WM) fiber bundle alterations in presumed limbic-predominant age-related TAR DNA-binding protein 43 encephalopathy (LATE) patients identified by isolated episodic/limbic amnesia, the absence of positive Alzheimer's disease (AD) biomarkers, and no other neurological diagnosis after 2 years of follow-up.

Michel Bottlaender and Marie Sarazin contributed equally to this work.

- Presumed LATE and amnestic AD shared similar patterns of WM alterations in fiber bundles of the limbic and temporal lobes, in congruence with their similar limbic cognitive phenotype.
- Presumed LATE differed from AD by the alteration of the callosal fibers connecting the middle frontal gyri and of the cerebello–thalamo–cortical tract.
- WM fiber bundle alterations were consistent with results on regional cortical atrophy.
- The different anatomical patterns of WM degeneration could provide information on the propagation pathways of distinct proteinopathies.

## 1 | BACKGROUND

Limbic-predominant age-related TAR DNA-binding protein 43 (TDP-43) encephalopathy (LATE) is a recently described entity, neuropathologically characterized by the aggregation and accumulation of abnormal neuronal TDP-43 protein with or without coexisting hippocampal sclerosis.[1,2] Clinically, this entity is characterized by a progressive amnestic syndrome, consistent with limbic/episodic amnesia, mimicking early Alzheimer's disease (AD).[3,4] While it is currently impossible to diagnose LATE in vivo with certainty, as TDP-43 in vivo biomarkers are not currently available, Nelson et al.[3] proposed to use a combination of biomarkers to rule in the diagnosis of LATE. In this perspective, the absence of positive AD biomarkers (plasma, cerebrospinal fluid (CSF), molecular positron emission tomography (PET) imaging) in individuals with isolated amnestic syndrome and medial temporal lobe atrophy would most likely signify LATE +/− hippocampal sclerosis.

Because AD and LATE have distinct underlying biological mechanisms leading to different therapeutic strategies, it is important to better understand how LATE differs from AD. A growing body of experimental evidence supports the hypothesis that neurodegenerative proteinopathies, such as amyloid, tau, or TDP-43, could share similar propagation mechanisms, such as the ability to spread from cell to cell within anatomically interconnected neurons, exhibiting prion-like properties.[5–7] The involvement of white matter (WM) fiber bundles in this propagation can be questioned: early WM alterations are observed in neurodegenerative diseases, marked by myelin degeneration and axonal loss.[8–10] In this context, investigating WM as an ensemble of fiber bundles connecting gray matter regions could provide crucial information for delineating the propagation pathways of specific proteinopathies.[11,12]

Diffusion magnetic resonance imaging (MRI) is a widely known technique that enables the study of WM fiber bundles in vivo. This technique has already been used to study AD in numerous works.[13–16] Recently, a technique called fixel-based analysis has been developed to analyze diffusion MRI at a within-voxel level. It is a state-of-the-art method that enables the characterization of multiple fiber orientations within voxels, providing information on the microstructure, with a measure of fiber density, and on the macrostructure, with a measure of fiber bundle atrophy.[17,18] This method overcomes a major confound of classic diffusion MRI models in the presence of crossing fibers, by defining a new basic element called fixel, representing one fiber population within a voxel. Metrics can then be derived for each fixel, enabling the definition of metrics specific to each fiber population, thus avoiding the confound that results from averaging fiber populations in voxel-based methods. This method has shown reliable results, notably for the study of AD.[19,20]

In the present study, for the first time to the best of our knowledge, we investigated WM fiber bundle alterations in presumed LATE and we explored how these alterations can differ from those in early AD, using fixel-based analysis. We included patients who all present an amnestic syndrome of the hippocampal type and strict pathophysiological criteria, including the positivity of AD pathophysiological markers (CSF biomarkers and both amyloid and tau PET imaging) for AD patients. Patients with presumed LATE were defined as a diagnosis of exclusion, by their amnestic limbic cognitive phenotype, the negativity of AD pathophysiological markers, and a 2-year clinical and MRI follow-up allowing to exclude another neurological diagnosis. Control subjects were also included. We first computed a whole-brain fixel-based analysis to explore differences between groups and identify WM tracts that are altered in each group. We then performed a tract-based analysis to further investigate the alteration of each identified tract in presumed LATE patients compared to controls and in AD patients for whom cognitive impairment was limited to an amnestic syndrome. Finally, we investigated regional cortical atrophy.

## 2 | METHODS

### 2.1 | Study participants

This study includes 64 participants from the SHATAU7-IMATAU cohort (EudraCT: 2015-000257-20). All subjects provided informed written consent. The study was approved by a French Ethics Committee (CPP Ile-de-France VI). All participants underwent complete clinical and neurological assessment, 3-tesla brain MRI, lumbar puncture for AD biomarker measures (except for controls), and [$^{11}$C]-Pittsburgh

**RESEARCH IN CONTEXT**

1. **Systematic review**: The authors reviewed the literature using traditional sources (e.g., PubMed). Prior studies using fixel-based analysis in Alzheimer's disease (AD) did not provide conclusive results on early stages of amnestic AD. White matter (WM) fiber bundle alterations have not yet been investigated in presumed limbic-predominant age-related TAR DNA-binding protein 43 encephalopathy (LATE) patients.
2. **Interpretation**: Presumed LATE and amnestic early AD shared similar temporal and limbic WM alterations. They differed by the involvement of both middle frontal callosal fibers and the cerebello–thalamo–cortical tract in presumed LATE. These results are consistent with regional cortical atrophy and with the staging system of the corresponding proteinopathies. It questions the possible association between WM alterations and the propagation of specific proteinopathies.
3. **Future directions**: Our findings revealed the alteration of specific WM fiber bundles in presumed LATE patients. Further studies in confirmed LATE are needed to better understand the role of these tracts and the regions they connect in the pathophysiology of the disease.

compound B PET imaging (missing data for 2 AD patients and 3 controls) and [$^{18}$F]-Flortaucipir PET imaging (missing data for 3 AD patients, 1 presumed LATE patient, and 3 controls), and were followed up annually with repeated standardized clinical and neuropsychological assessments for 2 years, including a second MRI at the last visit.

Patients with AD ($n$ = 27) at the stage of mild cognitive impairment or mild dementia were included according to clinical–biological criteria, including (1) predominant amnestic clinical phenotype of AD; (2) Clinical Dementia Rating (CDR) scale = 0.5 or 1; (3) AD CSF biomarkers suggestive of AD process (phosphorylated-tau/amyloid-beta 42 > 0.08);[21] (4) both positive amyloid PET (global cortical index > 1.45) and tau PET imaging (standardized uptake value ratio in a temporal meta volume of interest composed of the entorhinal cortices, parahippocampi, fusiform gyri, inferior and middle temporal cortices) when available, as described in a previous study.[22] In a subset of AD patients ($n$ = 20), cognitive impairment was limited to an amnestic syndrome of the hippocampal type, without alteration of parietal functions; they were therefore referred to as amnestic AD patients.

Patients with presumed LATE ($n$ = 18) were included according to the following criteria: (1) progressive amnestic syndrome of the hippocampal type; (2) CDR = 0.5 or 1; (3) CSF biomarkers not suggestive of AD; (4) negative amyloid PET and/or tau PET imaging;[22] (5) no extrapyramidal signs or other neurological signs suggestive of Parkinson's disease, progressive supranuclear palsy, corticobasal degeneration, frontotemporal dementia, dementia with Lewy bodies; and (6) absence of neurological diagnoses other than presumed LATE after 2 years of clinical follow-up, including a second MRI ($n$ = 13/18) and a second negative tau PET scan when available ($n$ = 12/18). Note that three patients had positive amyloid PET imaging despite normal CSF biomarkers and negative initial and longitudinal tau PET imaging. They were considered presumed LATE patients with amyloid copathology and included in the study.

Healthy controls ($n$ = 19) were recruited according to the following criteria: (1) Mini-Mental State Examination (MMSE) score ≥ 27/30 and normal neuropsychological assessment; (2) CDR = 0; (3) no memory complaints, or history of neurological or psychiatric disorders; and (4) negative amyloid and tau PET imaging when available.

Patients with (1) sleep apnea, (2) systemic illnesses that could interfere with cognitive functioning, (3) suspicion of alcohol or drug abuse, (4) history of psychiatric disorders, (5) history of stroke or severe cortical or subcortical vascular lesions, and (6) epilepsy were excluded.

## 2.2 | Image acquisition

MRI was acquired using a 3-tesla Siemens Magnetom Prisma scanner with a 64-channel coil. Data were acquired at the Paris Brain Institute (Centre de Neuroimagerie de Recherche, ICM, Paris). For each subject, diffusion-weighted images were acquired using a pulsed gradient spin echo single-shot echo planar imaging sequence with anteroposterior phase encoding (echo time (TE) = 77 ms, repetition time (TR) = 7s, voxel size = 1.3 mm isotropic, acquisition matrix = 184×184, 110 axial slices, multiband acceleration = 2, generalized autocalibrating partial parallel acquisition acceleration = 2, partial Fourier factor = 0.625). Using a partial Fourier factor enables us to decrease the echo time and therefore, to enhance the signal-to-noise ratio of the images, but it probably decreases the effective spatial resolution in the phase encoding direction. Each diffusion acquisition comprised three shells of diffusion with $b$-values of 200, 1700, and 4200 s/mm$^2$, with 60 directions per shell, and three volumes without diffusion weighting ($b$ = 0 s/mm$^2$). T1-weighted images were also acquired for each subject with a magnetization-prepared rapid acquisition gradient echo sequence (voxel size = 1 mm isotropic, TE = 2.15 ms, TR = 2400 ms, inversion time = 1000 ms, flip angle = 9°).

## 2.3 | Image preprocessing

T1-weighted images were controlled for quality visually, guided by MRIQC.[23] We then extracted the brain using HDBET[24] and registered these anatomical images onto the preprocessed diffusion-weighted images using the 'epi_reg' tool, which uses boundary-based registration,[25] from FMRIB's Software Library (FSL, version 6.0.5).[26] T1-weighted images were then processed using FreeSurfer 6.0.0 'recon-all' algorithm[27,28] to segment subcortical areas and parcellate the cortex with the Desikan–Killiany atlas[29] at the subject level. Results were visually inspected to identify global segmentation abnormalities and manual edits were performed on the brain mask

(pial surface errors) or on the WM volume (segmentation errors) when necessary. We then extracted the mean cortical thickness for the 68 cortical regions of the atlas to investigate regional cortical atrophy.

Preprocessing of diffusion-weighted images included visual quality control, denoising[30] using the 'dwidenoise' tool from MRtrix3 (version 3.0.2),[31] and dynamic correction of susceptibility-induced distortion artefacts, eddy current–induced distortions, and head motion, using the 'eddy_openmp' tool from FSL[32] with replacement of outliers[33] and susceptibility-by-movement correction options.[34] Prior to eddy, we used Synb0-DisCo[35] to estimate the susceptibility-induced distortion artefacts, due to the lack of a $B_0$ field map or blip-down acquisitions. We, therefore, used this algorithm on each acquired $b = 0$ volume to synthesize a corresponding undistorted $b = 0$ image, and we then performed the estimation using the 'topup' algorithm from FSL[36] and all reconstituted pairs of each subject. After eddy, we verified the quality of the data using the 'eddyqc' tool.[37]

We followed the fixel-based analysis pipeline recommended by the authors of the method,[17] unless otherwise stated. All steps were performed using commands implemented within MRtrix3 (version 3.0.2). The pipeline used is described in supporting information. We first obtained three-tissue response functions for each subject using the 'dhollander' algorithm[38] for the gray and white matter response functions and the 'msmt_5tt' algorithm[39] for the CSF response function, as this algorithm provided a better voxel selection for the CSF. Mean response functions of the healthy controls were used in the following. Analysis was performed at the native image resolution (1.3 mm isotropic). Fiber orientation distributions (FODs) were then estimated for each subject using multi-shell multi-tissue constrained spherical deconvolution.[39] Joint bias field correction and global intensity normalization of multi-tissue compartment parameters were applied to the results. A group-specific population FOD template was created using the FODs of 32 randomly selected participants (8 AD patients, 8 presumed LATE patients, and 16 healthy controls), and the FODs of each subject were then registered to the population template. We found that the default regularization parameters resulted in a suboptimal alignment, namely an extensive residual variability in ventricular size. As a result, we decided to decrease the regularization parameters, which successfully reduced the variability in ventricular size after registration. Despite this optimization, limited but observable registration inaccuracies remained in the periventricular area (between one and two voxels).

A brain mask of the template was then obtained by intersecting all subject masks in the template space. To minimize spurious results due to remaining periventricular registration inaccuracies, we additionally excluded from the mask the areas where the confusion between WM and CSF compartments among subjects was too extensive. Finally, we segmented the registered FODs from each subject into fixels and calculated the three metrics in each fixel: fiber density (FD), fiber bundle cross-section (FC), and combined fiber density and cross-section (FDC = FD × FC). These three metrics provide complementary information: FD can be interpreted as a relative measure of axonal density, FC provides a measure of macroscopic atrophy, and FDC captures the effects of fiber loss due to either reduction in fiber density and/or atrophy.

## 2.4 | Whole-brain fixel-based analysis

We first performed an exploratory whole-brain fixel-based analysis to identify tracts of interest without anatomical a priori. To do so, we generated a tractogram on the FOD template using probabilistic whole-brain tractography with twenty million fibers, which were subsequently filtered to two million fibers using the 'sift' algorithm.[40] For each of the three metrics, we tested for group differences using regularized fixel-wise statistical tests, which are described in more detail in Section 2.6 below. It allowed us to delineate brain areas where a statistically significant difference was found for at least one of the three metrics in at least one disease. We then identified the fiber bundles passing through these areas to compute tract-of-interest analyses.

## 2.5 | Tract-of-interest analyses: Identification and construction of the tracts

### 2.5.1 | Identification of tracts of interest

Based on the exploratory whole-brain fixel-based analysis, we identified 17 tracts encompassing all fixels that showed significant differences in either disease group. To do so, we first used TractSeg[41] on the FOD template, a deep-learning algorithm that performs automated segmentation of WM tracts. It allowed us to identify the inferior longitudinal fasciculi, uncinate fasciculi, and cingulum bundles. We then referred to the literature to identify the remaining bundles and we identified them as being: the temporopulvinar bundle of Arnold,[42–46] the cerebello–thalamo–cortical tract,[47] and the callosal fibers connecting (1) posterior segments of the superior frontal gyri, (2) caudal middle frontal gyri, and (3) precentral gyri. To identify the specific termination of the cerebello–thalamo–cortical tract, which connects to many cerebral areas from the prefrontal to the parietal cortices, we registered the mask of our results in the Montreal Neurological Institute space and referred to the Jülich Brain probabilistic atlas of the human brain's cytoarchitecture.[48] We identified that the fibers overlapping with significant fixels appeared to be going to the 6ma area of the Jülich Brain Atlas, which corresponds to the pre-supplementary motor area.

### 2.5.2 | Construction of tracts of interest

We computed the tractography on the FOD template of the inferior longitudinal and uncinate fasciculi using the beginning and ending masks provided by TractSeg, after checking that these masks were consistent with the description of these bundles.[49–51]

For each subject, we then transformed the segmentations and parcellations obtained from FreeSurfer into the common FOD template

space, and we computed probabilistic maps of presence for each region. The thresholded probabilistic maps of presence of the different regions were then used as beginning and ending regions for the tractography, on the FOD template, of the rest of the identified bundles cited above. These regions are summarized in Table S1 in supporting information. The cingulum was divided into dorsal and ventral parts.[52] Finally, the cerebello–thalamo–cortical tract was treated as a particular case, as we observed that the ending region of this bundle was only one segment of the superior frontal gyrus (presumably the pre-supplementary motor area). As the Desikan–Killiany atlas does not provide a subdivision of the superior frontal gyrus, we truncated this gyrus along the anteroposterior axis, leaving only the area connected to the fibers showing a high standard effect (Figure S1 in supporting information). The same truncated region was used for tractography of the callosal fibers connecting the bilateral posterior segments of the superior frontal gyri.

In summary, we reconstructed 17 bundles, directly on the common FOD template space, using the 'tckgen' and 'tckedit' tools of MRtrix3, namely: the bilateral inferior longitudinal fasciculi, uncinate fasciculi, dorsal cingula, ventral cingula, temporopulvinar bundles of Arnold, cerebello–thalamo–cortical tracts which we divided into cerebello–thalamic (inferior) and thalamo–cortical (superior) sections, the callosal fibers connecting the bilateral truncated superior frontal gyri, the callosal fibers connecting the bilateral caudal middle frontal gyri, and the callosal fibers connecting the bilateral precentral gyri. The anatomical descriptions of the beginning and ending regions of each identified tract are summarized in Table S1. We also reconstructed the fornices as they overlapped with the results of the whole-brain fixel-based analysis, but we decided not to include them in the tract of interest analyses as they were too close to the ventricles and therefore confounded by CSF partial volume effects.

## 2.6 | Statistical analyses

### 2.6.1 | Whole-brain fixel-based analysis

In the first exploratory whole-brain fixel-based analysis, we computed statistical tests for each metric FD, FC, and FDC, at each fixel, using a general linear model including age, sex, MMSE score, and intracranial volume (for the FC and FDC metrics only) as covariates, to compare (1) AD patients versus controls and (2) presumed LATE patients versus controls. Connectivity-based smoothing and statistical inference were performed using connectivity-based fixel enhancement[53] using default parameters and non-parametric permutations. The significance of the results was assessed using family-wise error correction with a type I error rate of 5%.

This first exploratory whole-brain analysis was meant to identify tracts of interest that we will then study in a future tract-based analysis. We therefore conducted it on the whole group of AD patients ($n = 27$).

### 2.6.2 | Tract of interest analyses

Based on the exploratory whole-brain fixel-based analysis, we identified and reconstructed on the common FOD template 17 tracts, and we performed tract-of-interest analyses. For each tract, we calculated the mean FD, FC, and FDC for the whole tract by taking the average of each metric over all fixels associated with the tract, weighted by track density. We performed statistical tests for each of the three metrics using a general linear model with age, sex, MMSE score, and intracranial volume (for the FC and FDC metrics only) as covariates, to compare (1) AD versus controls, (2) presumed LATE versus controls, and (3) AD versus presumed LATE. The significance of the results was assessed with one-sided *t* tests, performing false discovery rate correction among the 51 tests performed with a type I error rate of 5%. For each of the three metrics and each patient group, the results were presented as the mean metric with a 95% confidence interval, as a percentage difference with reference to the control mean value.

We performed these analyses on the subgroup of amnestic AD patients ($n = 20$) to ensure that the comparison between AD and presumed LATE was not biased by a difference in clinical phenotype and/or severity stage, and thus to generate a more characteristic spatial distribution of WM alterations depending on each pathophysiological process independently of the clinical phenotype. We verified that the results were not significantly modified when all AD patients ($n = 27$) were included.

### 2.6.3 | Regional cortical thickness

We performed region of interest analyses on mean regional cortical thicknesses extracted for each region of the Desikan–Killiany parcellation. For each of the 68 regions, we performed statistical tests using a general linear model with age, sex, and MMSE score as covariates to compare (1) amnestic AD versus controls, (2) presumed LATE versus controls, and (3) amnestic AD versus presumed LATE. The significance of the results was assessed with one-sided *t* tests, performing false discovery rate correction among the 204 tests performed with a type I error rate of 5%. For each patient group, the results were presented as a percentage difference with reference to the control mean value.

One amnestic AD patient was excluded from these analyses because of insufficient quality of the T1-weighted image.

## 3 | RESULTS

Demographic, clinical, and imaging data of amnestic AD patients, presumed LATE patients, and healthy controls are summarized in Table 1. Episodic memory deficit and hippocampal atrophy were similar between amnestic AD and presumed LATE patients. Presumed LATE patients were older than amnestic AD patients.

Characteristics of the whole AD group are available in Table S2 in supporting information.

**TABLE 1** Demographic, clinical, and imaging data of participants.

| | Amnestic AD ($n = 20$) | Presumed LATE ($n = 18$) | Controls ($n = 19$) | Statistics |
|---|---|---|---|---|
| ***Demographics*** | | | | |
| Age, years (SD) | 72.7 (5.5)* | 77.2 (5.4)* | 68.3 (4.6)* | $F = 12.9, p < 0.001$ |
| Males (%) | 10 (50) | 12 (67) | 6 (32)* | $X^2 = 12.2, p < 0.01$ |
| Years of education (SD) | 15.2 (4.2) | 14.4 (4.5) | 14.6 (3.0) | $F = 0.18, p = 0.84$ |
| ***Functional status*** | | | | |
| CDR (SD) | 0.6 (0.2) | 0.8 (0.4) | 0.0 (0.0)* | $F = 47.8, p < 0.001$ |
| ***Global cognitive efficiency*** | | | | |
| MMSE (SD) | 24.5 (3.2) | 24.4 (3.0) | 29.1 (0.8)* | $F = 19.1, p < 0.001$ |
| ***Verbal episodic memory*** | | | | |
| FCSRT—Free recall (SD) | 10.1 (7.4) | 9.7 (5.6) | 33.8 (4.6)* | $F = 95.3, p < 0.001$ |
| FCSRT—Total recall (SD) | 24.7 (10.8) | 27.0 (11.2) | 47.2 (1.0)* | $F = 34.0, p < 0.001$ |
| ***Visual episodic memory*** | | | | |
| Rey memory (SD) | 8.8 (4.9) | 8.2 (6.8) | 18.8 (5.7)* | $F = 18.9, p < 0.001$ |
| ***Molecular PET imaging*** | | | | |
| Amyloid PET SUVR GCI[a] (SD) | 2.86 (0.64)* | 1.40 (0.25) | 1.28 (0.10) | $F = 78.0, p < 0.001$ |
| Tau PET SUVR in a temporal meta-VOI[b] (SD) | 2.08 (0.74)* | 1.20 (0.10) | 1.22 (0.13) | $F = 20.9, p < 0.001$ |
| ***MRI*** | | | | |
| Intracranial volume (SD) | 1580 (159) | 1695 (182) | 1607 (116) | $F = 2.7, p = 0.08$ |
| Hipp volume (SD) | 1.94 (0.31) | 1.75 (0.34) | 2.46 (0.22)* | $F = 28.0, p < 0.001$ |
| Fazekas score (0/1/2/3) | 12/6/1/1 | 7/9/1/1 | 12/6/0/0 | – |

*Notes*: Mean values (standard deviation) or numbers (%) are presented for each data. Statistics report *p* values from one-way between-groups ANOVA for continuous variables and chi-squared tests for independence for categorical variables. Post hoc Tukey honest significance difference tests were then performed to compare each group to the others.

Abbreviations: CDR, Clinical Dementia Rating scale; FCSRT, Free and Cued Selective Reminding Test; GCI, Global Cortical Index; Hipp volume, hippocampal volumes normalized to intracranial volumes; MMSE, Mini-Mental State Examination; SD, standard deviation; SUVR, standardized uptake volume ratio; VOI, Volume Of Interest.

[a]Missing data for one AD patient and three control subjects.

[b]Missing data for two AD patients, one presumed LATE patient, and three control subjects; temporal meta-VOI composed of the entorhinal cortices, parahippocampi, fusiform gyri, inferior, and middle temporal cortices.

*$p < 0.05$ versus the other groups (assessed with two post hoc Tukey honest significance difference tests).

## 3.1 | Whole-brain fixel-based analysis

The results of the first exploratory whole-brain fixel-based analysis are shown in Figure 1 for the three metrics FDC, FD, and FC. We found distinct spatial distributions of WM fiber bundle alterations between the whole group of AD patients and presumed LATE patients. Alterations were mainly localized in the temporal and limbic lobes in AD (inferior longitudinal fasciculus, uncinate fasciculus, ventral and dorsal cingulum, temporopulvinar bundle of Arnold, fornix), and in fibers of the cerebello–thalamo–cortical tract and corpus callosum in presumed LATE.

## 3.2 | Tract-of-interest analyses

The 17 tracts identified as altered in Figure 1 were reconstructed by tractography. They are displayed in Figure 2. Figure 3 shows the results obtained for the comparisons between (1) amnestic AD patients versus controls, (2) presumed LATE patients versus controls, and (3) amnestic AD patients versus presumed LATE patients, for each metric FDC (Figure 3, graph A), FD (Figure 3, graph B), and FC (Figure 3, graph C). The results of the tract-of-interest analyses performed using the whole AD group ($n = 27$) are available in Figure S2 in supporting information.

The fiber density and cross-section (FDC) metric (Figure 3, graph A), which provides a measure sensitive to the number of fibers within the fiber bundle, was decreased in amnestic AD patients compared to controls in the right dorsal and ventral cingulum, temporopulvinar bundle of Arnold, and uncinate fasciculus, in the bilateral inferior longitudinal fasciculi, and in callosal fibers connecting the posterior superior frontal gyri. Moreover, we found a decrease in FDC in presumed LATE patients compared to controls in callosal fibers connecting the caudal middle frontal gyri, those connecting the posterior superior frontal gyri, in all parts of the cerebello–thalamo–cortical tracts (left and right, inferior and superior), and in the right ventral cingulum, temporopulvinar bundle of Arnold, inferior longitudinal fasciculus, and uncinate fasciculus. We did not find any significant difference

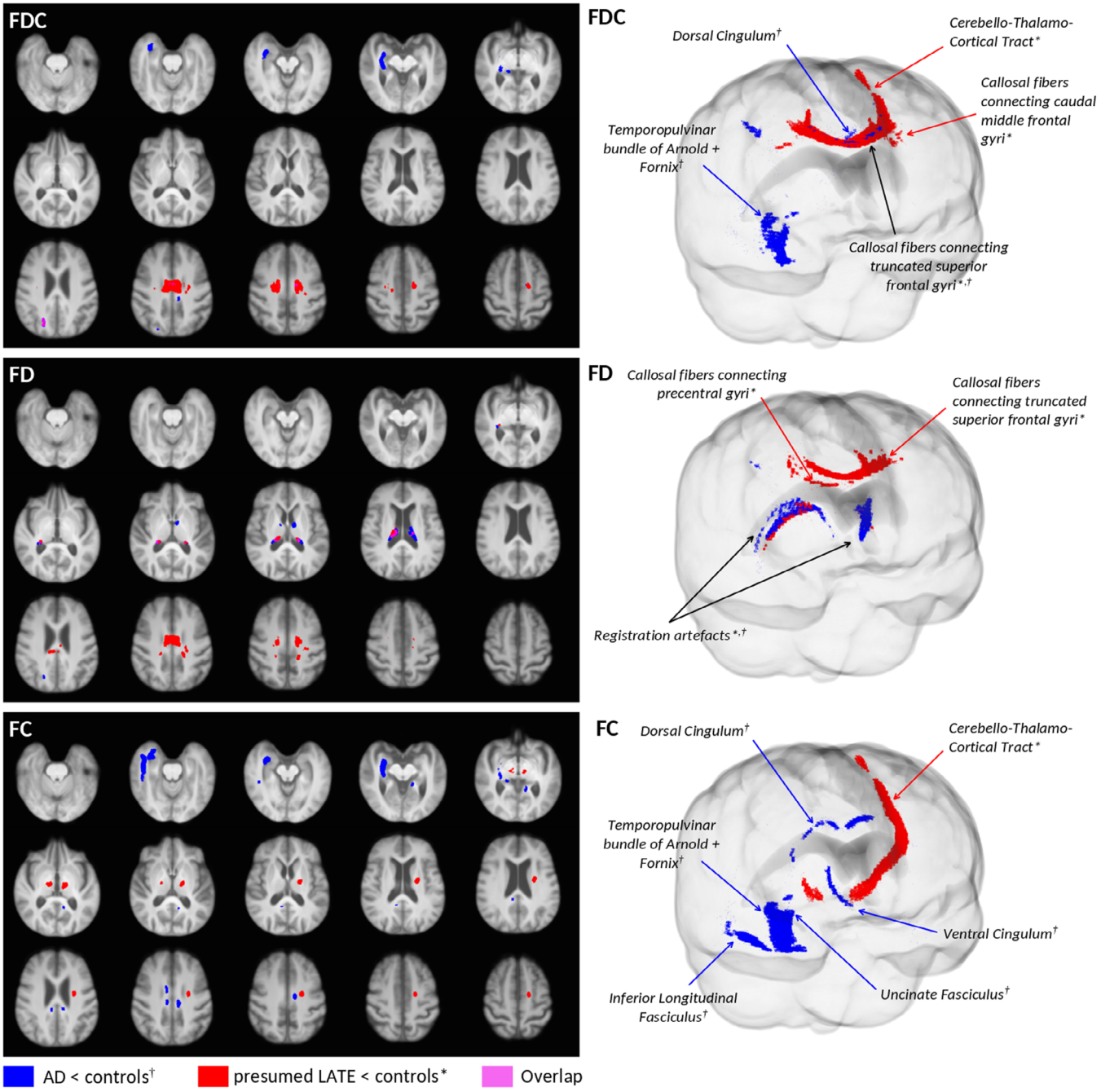


**FIGURE 1** Whole-brain fixel-based analysis: FDC, FD, and FC alterations observed for AD (blue†) and presumed LATE (red*) patients compared to healthy controls. Significant results ($p$ value < 0.05 after family-wise error correction) were obtained for the following three metrics: FDC, FD, and FC, in the whole-brain fixel-based analysis for the tests AD versus controls (blue†) and presumed LATE versus controls (red*). The pink shades correspond to the overlap areas between the results obtained for each comparison. Results are displayed as cropped fibers from the template-derived tractogram and are presented across axial slices of the mean T1-weighted image across all subjects (each T1-weighted image was previously registered on the FOD template) on the left panel, and through a glass brain representation on the right panel to help visualize the pathways.

in the direct comparison between amnestic AD and presumed LATE patients.

The FDC metric, being a composite metric obtained as the product of FD by FC, is therefore sensitive to fiber loss both at the microscopic scale (fiber density reduction) and at the macroscopic scale (bundle atrophy). After reporting the results obtained for FDC, it is interesting to observe for each altered tract whether this alteration is driven more by fiber density reduction or by fiber bundle atrophy. The results obtained for the FD and FC metrics are shown in Figure 3, graphs B and C. We observed that, in amnestic AD patients, alterations of the cingulum and the temporopulvinar bundle of Arnold are driven more by a reduction in fiber bundle cross-section (atrophy), whereas alterations in the uncinate fasciculus and in callosal fibers are driven more by a reduction in fiber density. In this disease, alterations in the inferior

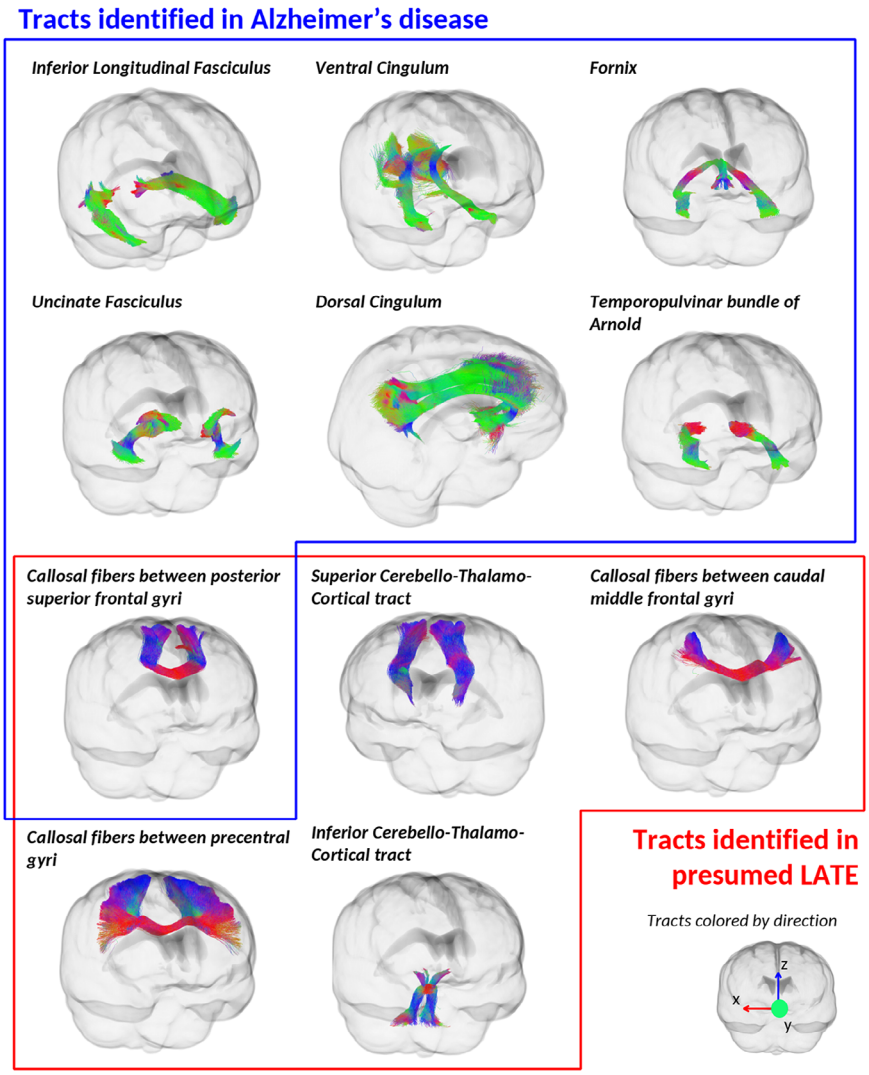


**FIGURE 2** Reconstruction of the tracts identified as altered in at least one of the tests in the whole-brain fixel-based analysis displayed through glass brains. The tracts are colored according to fiber directions (green: anteroposterior axis, blue: inferior–superior axis, red: left–right axis). Glass brains are circled according to the comparison for which the tract showed a statistically significant alteration in the whole-brain fixel-based analysis: in blue for the comparison between AD and controls, and in red for the comparison between presumed LATE and controls.

longitudinal fasciculus are due to both fiber density and fiber bundle cross-section reduction, with the reduction of fiber bundle cross-section being larger. In presumed LATE patients, we observed that alterations in the cerebello–thalamo–cortical tract, callosal fibers, and temporopulvinar bundles of Arnold are driven more by atrophy, whereas alterations in the ventral cingulum, inferior longitudinal fasciculus, and uncinate fasciculus are driven more by fiber density reduction.

In the direct comparison between the two groups of patients, we found a significant reduction in FD in presumed LATE patients compared to amnestic AD patients in callosal fibers connecting precentral gyri. We also found a significant reduction in FC in presumed LATE patients compared to amnestic AD patients in the left inferior part of the cerebello–thalamo–cortical tract.

### 3.3 | Regional cortical thickness

The results of the regional cortical thickness analysis are shown in Figure 4. Cortical thickness was reduced in almost all temporal regions in amnestic AD patients compared to healthy controls: entorhinal cortex; fusiform gyrus; inferior, middle, and superior temporal gyri; transverse temporal gyrus; and temporal pole. Cortical thickness was also reduced in amnestic AD patients compared to controls in occipital regions: lingual gyrus and lateral occipital cortex; parietal regions: precuneus, inferior parietal, and supramarginal gyri; in the insula; and in frontal regions: superior and caudal middle frontal gyri. In presumed LATE patients, cortical thickness was reduced compared to controls in the entorhinal cortex, in frontal regions: superior frontal gyrus, rostral and caudal middle frontal gyrus, parsopercularis, parstriangularis, and parsorbitalis gyri, and in supramarginal gyrus. No significant differences were observed in the direct comparison between amnestic AD and presumed LATE patients.

## 4 | DISCUSSION

In this study, we investigated for the first time, to the best of our knowledge, WM alterations using a fixel-based analysis in presumed LATE patients, who were defined by an episodic memory impairment

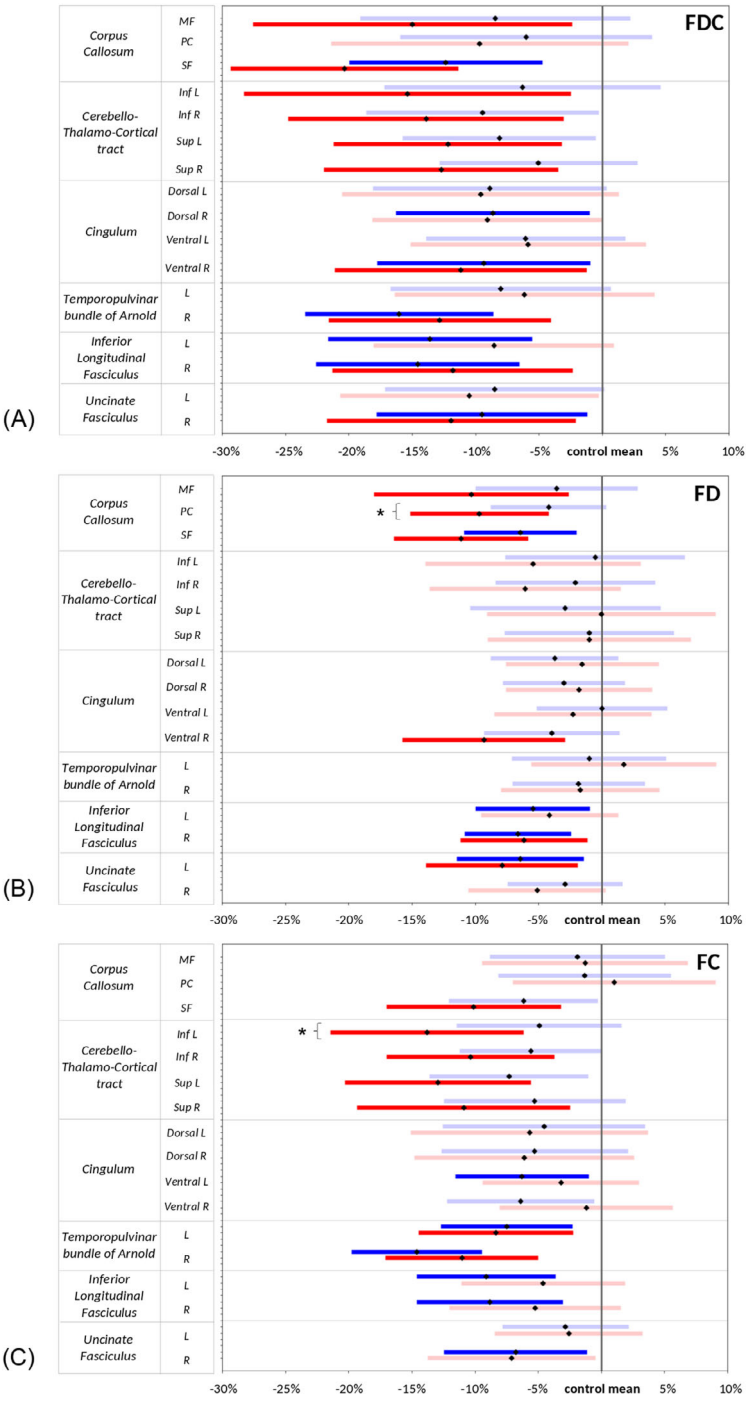


**FIGURE 3** Tract-of-interest analyses: significant decreases in FDC, FD, and FC in amnestic AD and presumed LATE patients compared to controls in selected tracts of interest. (A) FDC results, (B) FD results, and (C) FC results. For each metric and each tract, the mean metric in the patient group, as a percentage difference with controls, is represented with diamonds and confidence intervals at 95% with lines. For each tract, the first lines are colored in blue for the comparison between amnestic AD and controls and second lines in red for the comparison between presumed LATE and controls. Brighter colors highlight significant differences between patients and controls ($p < 0.05$ after false discovery rate correction). Stars highlight significant differences between amnestic AD and presumed LATE. Inf, inferior; L, left; MF, middle frontal gyrus; PC, precentral gyrus; R, right; SF, superior frontal gyrus

mimicking early AD, the absence of positivity of AD biomarkers, and the absence of other neurological diagnosis after 2 years of follow-up. By comparing the WM alterations in presumed LATE and amnestic early AD, we aimed to test the hypothesis that, despite similar clinical phenotypes, each disease alters WM differently. We found that both amnestic AD and presumed LATE patients showed WM alterations in tracts of the temporal and limbic lobes and in callosal fibers connecting superior frontal gyri. In addition, presumed LATE patients showed WM alterations in callosal fibers connecting the middle frontal gyri and in fibers of the cerebello–thalamo–cortical tract that terminates close to the pre-supplementary motor area. Investigating cortical thickness, we found that amnestic AD patients exhibited cortical atrophy mainly localized in the temporal and parietal lobes, with the entorhinal cortex being the most atrophied region compared to controls, while presumed LATE patients exhibited cortical atrophy mainly localized in the entorhinal cortex and in the frontal lobe, the entorhinal cortex also being the most atrophied region compared to controls. These regions correspond to the regions connected by the most altered WM tracts in each group.

In early amnestic AD, we found alterations of WM fiber bundles in the ventral cingulum, the inferior longitudinal fasciculus, the uncinate fasciculus, and in callosal fibers connecting the posterior superior

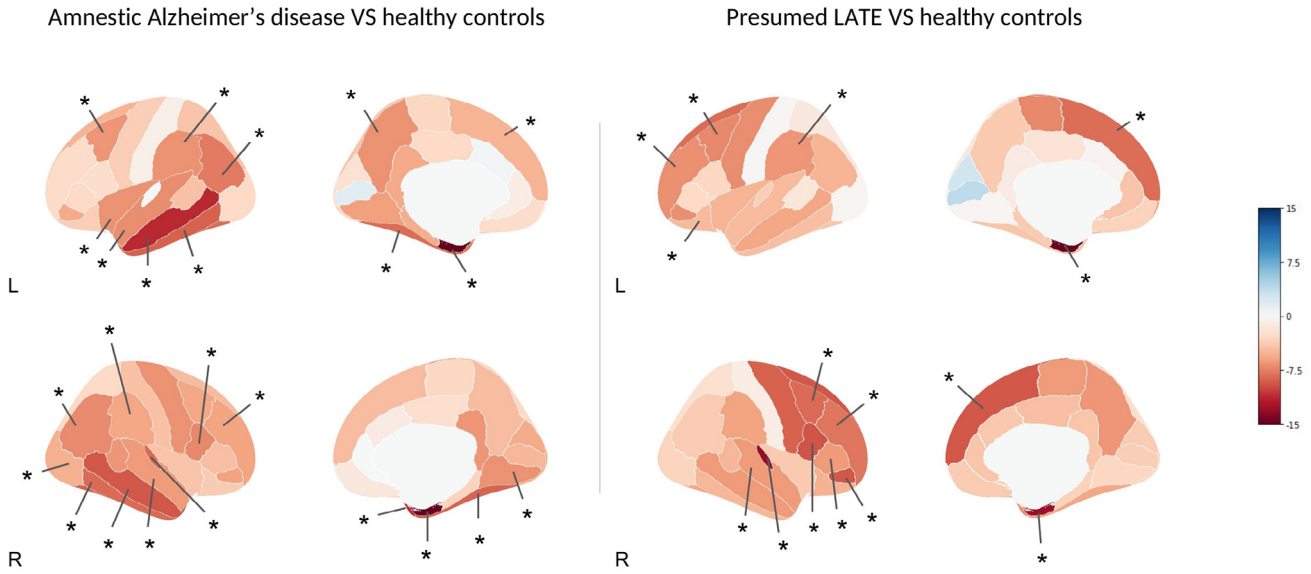


**FIGURE 4** Region of interest analyses on cortical thickness: significant decreases in cortical thickness in amnestic AD (left) and presumed LATE patients (right) compared to controls in all cortical regions of the Desikan–Killiany atlas. For each region and each comparison, the mean cortical thickness is represented with a color code on the corresponding region on the inflated surface of the FreeSurfer fsaverage brain, as a percentage difference with controls. Stars highlight significant differences between amnestic AD and controls, or between presumed LATE and controls ($p < 0.05$ after false discovery rate correction).

frontal gyri. These results are consistent with previous studies using various diffusion MRI methods.[13–16,19,20] Two previous studies used fixel-based analysis to explore WM fiber bundles in AD. Mito et al.[19] included patients at more advanced stages than those in our cohort, in whom we observed more restricted topographical tract damage in the temporal and limbic cortex. Surprisingly, Mito et al. did not find significant results in the group of 20 amyloid-positive patients with mild cognitive impairment, possibly because of the lack of strict cognitive inclusion criteria, resulting in a group of patients with high heterogeneity, as the authors themselves acknowledged. Dewenter et al.[20] did not take into account clinical status, making it difficult to interpret their results. Our study is, therefore, the first fixel-based analysis to obtain results on WM fiber bundle alterations in a group of early-stage AD patients. It confirms that fiber bundles of the temporal and limbic lobes are the primary deteriorated bundles in AD.

Interestingly, the different bundles observed as altered in the amnestic AD group connect regions that presented cortical atrophy, and that are known to present hyperphosphorylated tau aggregation: the ventral cingulum, inferior longitudinal fasciculus, and uncinate fasciculus connect the temporal lobe to the cingulate, occipital, and orbitofrontal cortices, respectively, all of which are included in the Braak staging system.[54,55]

Finally, we also highlighted the alteration of the temporopulvinar bundle of Arnold, a tract that, to our knowledge, has not been described in the AD diffusion MRI literature to date. This tract, initially identified as connecting the anterior temporal lobe to the pulvinar nucleus of the thalamus,[43] has subsequently been described as also connecting the presubiculum to the lateral dorsal nucleus of the thalamus and to some extent to the anterior nuclei.[45,46,56,57] The involvement of the temporopulvinar bundle at the early amnestic stage of AD is congruent with neuropathological data, showing that the thalamus, particularly the lateral dorsal nucleus, is affected by neurofibrillary tangles at the same stage as the hippocampus.[58,59] In addition, these regions are involved in the system of recollection memory,[60] which is affected in typical AD. In conclusion, finding WM alterations in the temporopulvinar bundle of Arnold could be new reliable and interesting information in the study of AD.

We defined presumed LATE patients, albeit as a diagnosis of exclusion, by strict clinical (isolated amnesia) and pathophysiological criteria (negativity of CSF AD biomarkers, and negativity of amyloid and/or tau PET imaging), as well as the absence of other diagnoses after 2 years of follow-up.[22] As expected, patients with presumed LATE were older than those with AD.[2]

To our knowledge, this study is the first diffusion MRI analysis conducted in presumed LATE patients. We found WM fiber bundle alterations not only in the same temporal and limbic tracts as in amnestic AD, but also in the cerebello–thalamo–cortical tract and in more spatially extended callosal fibers. These alterations occurring in tracts connecting regions of the frontal lobe are in agreement with results on cortical atrophy as we found that presumed LATE patients exhibited cortical atrophy in the entorhinal cortex and in many regions of the frontal lobe, including the superior and middle frontal gyri.

As both groups of amnestic AD and presumed LATE patients had a similar clinical phenotype but distinct causal proteinopathies, we hypothesize that the differences observed in WM fiber bundle alterations between the two groups of patients could be explained by the different pathophysiological processes. The spread of abnormal TDP-43 during the course of LATE is still under investigation. The consensus working group reports[2,61] established the following stages for the propagation of abnormal TDP-43 in the brain: TDP-43 deposition

begins in the amygdala (stage 1), followed by the hippocampus (stage 2), and finally reaches the middle frontal gyrus (stage 3). More detailed stages have been described by Nag et al.[1] and Young et al.[62] deriving an empirical staging system from data-driven disease progression modeling.

We found congruence between those regions sensitive to the accumulation of abnormal TDP-43 proteins and the fiber bundles that we identified as being altered in presumed LATE. Accumulation of abnormal TDP-43 has been reported in the beginning and ending regions of most of the fiber bundles identified in this study as altered in presumed LATE. We can for example mention the anterior temporal pole[1] and the prefrontal cortex,[1] which are structurally connected by the uncinate fasciculus. The temporopulvinar bundle of Arnold and the ventral cingulum are two limbic fiber bundles implicated in the recollection memory system for which we can also find congruence between their beginning and ending regions and deposition of abnormal TDP-43.[1,62] The alteration of the cerebello–thalamo–cortical tract was more surprising. This tract passes through the red nucleus, the lateral ventral nucleus of the thalamus, and the superior frontal gyrus near the pre-supplementary motor area. These regions are mentioned in staging systems of amyotrophic lateral sclerosis and frontotemporal dementia, two neurodegenerative diseases also associated with abnormal TDP-43 spreading.[63,64] Further studies are needed to confirm and investigate the role of these regions as potential regions of interest in LATE.

Despite the difficulty of comparing two pathologies that can sometimes occur simultaneously in the same patient, the present study advances the distinction between AD and presumed LATE by describing different white matter alterations in each disease that are congruent with their different pathological features and could contribute to a better understanding of their mechanisms. However, the purpose of this study is not to propose a diagnostic tool that could be used to differentiate AD from presumed LATE, as future studies will be needed to better understand the origins of these differences and to confirm that they are accurate on a subject level and not only on the group level.

One strength of this study is that the patient groups were very precisely defined in terms of clinical phenotype and relevant pathophysiological biomarkers. For the early amnestic AD group, this could explain why we found significant fiber bundle alterations with a number of patients similar to Mito et al.[19] Moreover, patients from both disease groups had similar phenotypes (neuropsychological scores and degree of hippocampal atrophy) and were therefore comparable in terms of disease severity.

Our study has several limitations, in particular the small sample size and the lack of neuropathological confirmation for presumed LATE. In the absence of specific biomarkers, the presumed LATE group is consistent with the definition of the disease given by the consensus working group report on LATE.[1–3,61] Moreover, in the situation in which the presumed LATE group we included would not exactly overlap with the pathophysiological definition of LATE, studying WM alterations in this clinically very homogenous group of individuals that present an amnestic syndrome of the hippocampal type and does not correspond to any other known diagnoses, is of high interest to better understand this disorder and the differences it presents with early AD. In addition, the presence of TDP-43 co-pathology in AD patients cannot be excluded.[1,3]

From a methodological point of view, we can highlight a limitation of the fixel-based method, which is highly dependent on the registration accuracy of the FODs to the template, whereas perfect registration between patients and controls with broad anatomical differences is difficult to achieve. To minimize biases due to this effect, we optimized the registration parameters and removed from the template brain mask the regions in which we could detect residual misregistration. As in previous fixel-based analysis studies,[19,20] and despite the special efforts we made, this prevented us from investigating the fornix, which would have been of great interest.

In conclusion, this study shows that, in agreement with their shared limbic clinical phenotype, AD and presumed LATE have similar anatomical patterns of WM degeneration in fiber bundles of the limbic and temporal lobes, like the temporopulvinar bundle of Arnold, the ventral cingulum, and the uncinate fasciculus. Furthermore, we found distinct WM alterations more specific to each disease. This is the case in the cerebello–thalamo–cortical tract and the callosal fibers connecting the middle frontal gyri, which are significantly altered in presumed LATE. These alterations of tracts connecting frontal regions are in agreement with the predominance of cortical atrophy in these same regions. Further studies on larger cohorts are needed to confirm these results and to investigate the relationship between these alterations and the underlying pathophysiologies.

## ACKNOWLEDGMENTS

We are grateful to the staff of the Centre de Neuroimagerie de Recherche (CENIR), Salpêtrière Hospital, for patient management during MRI acquisition, and to the chemical/radiopharmaceutical and nursing staff of the Service Hospitalier Frederic Joliot for the synthesis of [$^{11}$C]-PIB and [$^{18}$F]-Flortaucipir and for patient management, respectively. We are also indebted to AVID Radiopharmaceuticals, Inc. for their support in supplying the Flortaucipir precursor and chemistry production advice. Funding was provided by French Ministry of Health grant (PHRC-2013-0919 and PHRC- 0054-N 2010), CEA, Fondation pour la recherche sur la maladie d'Alzheimer, Institut de Recherches Internationales Servier, Fondation France-Alzheimer, and Institut Roche de Recherche et Médecine Translationnelle.

## CONFLICT OF INTEREST STATEMENT

The authors report no conflicts of interest. Author disclosures are available in the supporting information.

## CONSENT STATEMENT

All subjects provided informed written consent. The study was approved by a French Ethics Committee (CPP Ile-de-France VI).

## ORCID

*Aurélie Lebrun* https://orcid.org/0009-0002-6168-8964

## REFERENCES


1. Nag S, Schneider JA. Limbic-predominant age-related TDP43 encephalopathy (LATE) neuropathological change in neurodegenerative diseases. *Nat Rev Neurol*. 2023;19(9):525-541. doi:10.1038/s41582-023-00846-7
2. Nelson PT, Dickson DW, Trojanowski JQ, et al. Limbic-predominant age-related TDP-43 encephalopathy (LATE): consensus working group report. *Brain*. 2019;142(6):1503-1527. doi:10.1093/brain/awz099
3. Nelson PT, Schneider JA, Jicha GA, Duong MT, Wolk DA. When Alzheimer's is LATE: why does it matter? *Ann Neurol*. 2023;94(2):211-222. doi:10.1002/ana.26711
4. Duong MT, Wolk DA. Limbic-predominant age-related TDP-43 encephalopathy: LATE-breaking updates in clinicopathologic features and biomarkers. *Curr Neurol Neurosci Rep*. 2022;22(11):689-698. doi:10.1007/s11910-022-01232-4
5. Brettschneider J, Tredici KD, Lee VMY, Trojanowski JQ. Spreading of pathology in neurodegenerative diseases: a focus on human studies. *Nat Rev Neurosci*. 2015;16(2):109-120. doi:10.1038/nrn3887
6. Goedert M. Alzheimer's and Parkinson's diseases: the prion concept in relation to assembled Aβ, tau, and α-synuclein. *Science*. 2015;349(6248):1255555. doi:10.1126/science.1255555
7. Jucker M, Walker LC. Self-propagation of pathogenic protein aggregates in neurodegenerative diseases. *Nature*. 2013;501(7465):45-51. doi:10.1038/nature12481
8. Brun A, Englund E. A white matter disorder in dementia of the Alzheimer type: a pathoanatomical study. *Ann Neurol*. 1986;19(3):253-262. doi:10.1002/ana.410190306
9. McAleese KE, Walker L, Graham S, et al. Parietal white matter lesions in Alzheimer's disease are associated with cortical neurodegenerative pathology, but not with small vessel disease. *Acta Neuropathol (Berl)*. 2017;134(3):459-473. doi:10.1007/s00401-017-1738-2
10. Nasrabady SE, Rizvi B, Goldman JE, Brickman AM. White matter changes in Alzheimer's disease: a focus on myelin and oligodendrocytes. *Acta Neuropathol Commun*. 2018;6(1):22. doi:10.1186/s40478-018-0515-3
11. Wen Q, Risacher SL, Xie L, et al. Tau-related white-matter alterations along spatially selective pathways. *NeuroImage*. 2021;226:117560. doi:10.1016/j.neuroimage.2020.117560
12. Tian J, Raghavan S, Reid RI, et al. White matter degeneration pathways associated with tau deposition in alzheimer disease. *Neurology*. 2023;100(22):e2269-e2278. doi:10.1212/WNL.0000000000207250
13. Chen Y, Wang Y, Song Z, Fan Y, Gao T, Tang X. Abnormal white matter changes in Alzheimer's disease based on diffusion tensor imaging: a systematic review. *Ageing Res Rev*. 2023;87:101911. doi:10.1016/j.arr.2023.101911
14. Dang C, Wang Y, Li Q, Lu Y. Neuroimaging modalities in the detection of Alzheimer's disease-associated biomarkers. *Psychoradiology*. 2023;3:kkad009. doi:10.1093/psyrad/kkad009
15. Kamagata K, Andica C, Kato A, et al. Diffusion magnetic resonance imaging-based biomarkers for neurodegenerative diseases. *Int J Mol Sci*. 2021;22(10):5216. doi:10.3390/ijms22105216
16. Gold BT, Johnson NF, Powell DK, Smith CD. White matter integrity and vulnerability to Alzheimer's disease: preliminary findings and future directions. *Biochim Biophys Acta BBA—Mol Basis Dis*. 2012;1822(3):416-422. doi:10.1016/j.bbadis.2011.07.009
17. Dhollander T, Clemente A, Singh M, et al. Fixel-based analysis of diffusion MRI: methods, applications, challenges and opportunities. *NeuroImage*. 2021;241:118417. doi:10.1016/j.neuroimage.2021.118417
18. Raffelt DA, Tournier JD, Smith RE, et al. Investigating white matter fibre density and morphology using fixel-based analysis. *NeuroImage*. 2017;144:58-73. doi:10.1016/j.neuroimage.2016.09.029
19. Mito R, Raffelt D, Dhollander T, et al. Fibre-specific white matter reductions in Alzheimer's disease and mild cognitive impairment. *Brain*. 2018;141(3):888-902. doi:10.1093/brain/awx355
20. Dewenter A, Jacob MA, Cai M, et al. Disentangling the effects of Alzheimer's and small vessel disease on white matter fibre tracts. *Brain*. 2023;146(2):678-689. doi:10.1093/brain/awac265
21. Duits FH, Teunissen CE, Bouwman FH, et al. The cerebrospinal fluid "Alzheimer profile": easily said, but what does it mean? *Alzheimers Dement*. 2014;10(6):713-723.e2. doi:10.1016/j.jalz.2013.12.023
22. Lagarde J, Olivieri P, Tonietto M, et al. Distinct amyloid and tau PET signatures are associated with diverging clinical and imaging trajectories in patients with amnestic syndrome of the hippocampal type. *Transl Psychiatry*. 2021;11(1):1-10. doi:10.1038/s41398-021-01628-9
23. Esteban O, Birman D, Schaer M, Koyejo OO, Poldrack RA, Gorgolewski KJ. MRIQC: advancing the automatic prediction of image quality in MRI from unseen sites. *PLOS ONE*. 2017;12(9):e0184661. doi:10.1371/journal.pone.0184661
24. Isensee F, Schell M, Pflueger I, et al. Automated brain extraction of multisequence MRI using artificial neural networks. *Hum Brain Mapp*. 2019;40(17):4952-4964. doi:10.1002/hbm.24750
25. Greve DN, Fischl B. Accurate and robust brain image alignment using boundary-based registration. *NeuroImage*. 2009;48(1):63-72. doi:10.1016/j.neuroimage.2009.06.060
26. Smith SM, Jenkinson M, Woolrich MW, et al. Advances in functional and structural MR image analysis and implementation as FSL. *NeuroImage*. 2004;23:S208-S219. doi:10.1016/j.neuroimage.2004.07.051
27. Fischl B, Salat DH, Busa E, et al. Whole brain segmentation: automated labeling of neuroanatomical structures in the human brain. *Neuron*. 2002;33(3):341-355. doi:10.1016/S0896-6273(02)00569-X
28. Fischl B, van der Kouwe A, Destrieux C, et al. Automatically parcellating the human cerebral cortex. *Cereb Cortex*. 2004;14(1):11-22. doi:10.1093/cercor/bhg087
29. Desikan RS, Ségonne F, Fischl B, et al. An automated labeling system for subdividing the human cerebral cortex on MRI scans into gyral based regions of interest. *NeuroImage*. 2006;31(3):968-980. doi:10.1016/j.neuroimage.2006.01.021
30. Veraart J, Novikov DS, Christiaens D, Ades-aron B, Sijbers J, Fieremans E. Denoising of diffusion MRI using random matrix theory. *NeuroImage*. 2016;142:394-406. doi:10.1016/j.neuroimage.2016.08.016
31. Tournier JD, Smith R, Raffelt D, et al. MRtrix3: a fast, flexible and open software framework for medical image processing and visualisation. *NeuroImage*. 2019;202:116137. doi:10.1016/j.neuroimage.2019.116137
32. Andersson JLR, Sotiropoulos SN. An integrated approach to correction for off-resonance effects and subject movement in diffusion MR imaging. *NeuroImage*. 2016;125:1063-1078. doi:10.1016/j.neuroimage.2015.10.019
33. Andersson JLR, Graham MS, Zsoldos E, Sotiropoulos SN. Incorporating outlier detection and replacement into a non-parametric framework for movement and distortion correction of diffusion MR images. *NeuroImage*. 2016;141:556-572. doi:10.1016/j.neuroimage.2016.06.058
34. Andersson JLR, Graham MS, Drobnjak I, Zhang H, Campbell J. Susceptibility-induced distortion that varies due to motion: correction in diffusion MR without acquiring additional data. *NeuroImage*. 2018;171:277-295. doi:10.1016/j.neuroimage.2017.12.040
35. Schilling KG, Blaber J, Hansen C, et al. Distortion correction of diffusion weighted MRI without reverse phase-encoding scans or field-maps. *PLOS ONE*. 2020;15(7):e0236418. doi:10.1371/journal.pone.0236418
36. Andersson JLR, Skare S, Ashburner J. How to correct susceptibility distortions in spin-echo echo-planar images: application to diffusion tensor imaging. *NeuroImage*. 2003;20(2):870-888. doi:10.1016/S1053-8119(03)00336-7
37. Bastiani M, Cottaar M, Fitzgibbon SP, et al. Automated quality control for within and between studies diffusion MRI data using a

non-parametric framework for movement and distortion correction. *NeuroImage*. 2019;184:801-812. doi:10.1016/j.neuroimage.2018.09.073

38. Dhollander T, Mito R, Raffelt D, Connelly A. Improved white matter response function estimation for 3-tissue constrained spherical deconvolution. *Proc Intl Soc Mag Reson Med*. 2019; 27:555.
39. Jeurissen B, Tournier JD, Dhollander T, Connelly A, Sijbers J. Multi-tissue constrained spherical deconvolution for improved analysis of multi-shell diffusion MRI data. *NeuroImage*. 2014;103:411-426. doi:10.1016/j.neuroimage.2014.07.061
40. Smith RE, Tournier JD, Calamante F, Connelly A. SIFT: spherical-deconvolution informed filtering of tractograms. *NeuroImage*. 2013;67:298-312. doi:10.1016/j.neuroimage.2012.11.049
41. Wasserthal J, Neher P, Maier-Hein KH. TractSeg—fast and accurate white matter tract segmentation. *NeuroImage*. 2018;183:239-253. doi:10.1016/j.neuroimage.2018.07.070
42. Schmahmann J, Pandya D, Schmahmann J, Pandya D. *Fiber Pathways of the Brain*. Oxford University Press; 2010.
43. Klingler J, Gloor P. The connections of the amygdala and of the anterior temporal cortex in the human brain. *J Comp Neurol*. 1960;115(3):333-369. doi:10.1002/cne.901150305
44. Weiss A, Di Carlo DT, Di Russo P, et al. Microsurgical anatomy of the amygdaloid body and its connections. *Brain Struct Funct*. 2021;226(3):861-874. doi:10.1007/s00429-020-02214-3
45. Saunders RC, Mishkin M, Aggleton JP. Projections from the entorhinal cortex, perirhinal cortex, presubiculum, and parasubiculum to the medial thalamus in macaque monkeys: identifying different pathways using disconnection techniques. *Exp Brain Res*. 2005;167(1):1-16. doi:10.1007/s00221-005-2361-3
46. Nishio Y, Hashimoto M, Ishii K, et al. Multiple thalamo-cortical disconnections in anterior thalamic infarction: implications for thalamic mechanisms of memory and language. *Neuropsychologia*. 2014;53:264-273. doi:10.1016/j.neuropsychologia.2013.11.025
47. Palesi F, Tournier JD, Calamante F, et al. Contralateral cerebello-thalamo-cortical pathways with prominent involvement of associative areas in humans in vivo. *Brain Struct Funct*. 2015;220(6):3369-3384. doi:10.1007/s00429-014-0861-2
48. Amunts K, Mohlberg H, Bludau S, Zilles K. Julich-Brain: a 3D probabilistic atlas of the human brain's cytoarchitecture. *Science*. 2020;369(6506):988-992. doi:10.1126/science.abb4588
49. Catani M. The connectional anatomy of the temporal lobe. In: Miceli G, Bartolomeo P, Navarro V, eds. *Handbook of Clinical Neurology. The Temporal Lobe*. Elsevier; 2022:3-16. doi:10.1016/B978-0-12-823493-8.00001-8
50. Von Der Heide RJ, Skipper LM, Klobusicky E, Olson IR. Dissecting the uncinate fasciculus: disorders, controversies and a hypothesis. *Brain*. 2013;136(6):1692-1707. doi:10.1093/brain/awt094
51. Herbet G, Zemmoura I, Duffau H. Functional anatomy of the inferior longitudinal fasciculus: from historical reports to current hypotheses. *Front Neuroanat*. 2018;12:77. doi:10.3389/fnana.2018.00077
52. Bubb EJ, Metzler-Baddeley C, Aggleton JP. The cingulum bundle: anatomy, function, and dysfunction. *Neurosci Biobehav Rev*. 2018;92:104-127. doi:10.1016/j.neubiorev.2018.05.008
53. Raffelt DA, Smith RE, Ridgway GR, et al. Connectivity-based fixel enhancement: whole-brain statistical analysis of diffusion MRI measures in the presence of crossing fibres. *NeuroImage*. 2015;117:40-55. doi:10.1016/j.neuroimage.2015.05.039
54. Braak H, Braak E. Neuropathological stageing of Alzheimer-related changes. *Acta Neuropathol (Berl)*. 1991;82(4):239-259. doi:10.1007/BF00308809
55. Braak H, Alafuzoff I, Arzberger T, Kretzschmar H, Del Tredici K. Staging of Alzheimer disease-associated neurofibrillary pathology using paraffin sections and immunocytochemistry. *Acta Neuropathol (Berl)*. 2006;112(4):389-404. doi:10.1007/s00401-006-0127-z
56. Aggleton JP, Desimone R, Mishkin M. The origin, course, and termination of the hippocampothalamic projections in the macaque. *J Comp Neurol*. 1986;243(3):409-421. doi:10.1002/cne.902430310
57. Aggleton JP, Saunders RC. The relationships between temporal lobe and diencephalic structures implicated in anterograde amnesia. *Memory*. 1997;5(1-2):49-72. doi:10.1080/741941143
58. Braak H, Braak E. Alzheimer's disease affects limbic nuclei of the thalamus. *Acta Neuropathol (Berl)*. 1991;81(3):261-268. doi:10.1007/BF00305867
59. Aggleton JP, Pralus A, Nelson AJD, Hornberger M. Thalamic pathology and memory loss in early Alzheimer's disease: moving the focus from the medial temporal lobe to Papez circuit. *Brain*. 2016;139(7):1877-1890. doi:10.1093/brain/aww083
60. Carlesimo GA, Lombardi MG, Caltagirone C, Barban F. Recollection and familiarity in the human thalamus. *Neurosci Biobehav Rev*. 2015;54:18-28. doi:10.1016/j.neubiorev.2014.09.006
61. Nelson PT, Lee EB, Cykowski MD, et al. LATE-NC staging in routine neuropathologic diagnosis: an update. *Acta Neuropathol (Berl)*. 2023;145(2):159-173. doi:10.1007/s00401-022-02524-2
62. Young AL, Vogel JW, Robinson JL, et al. Data-driven neuropathological staging and subtyping of TDP-43 proteinopathies. *Brain*. 2023;146(7):2975-2988. doi:10.1093/brain/awad145
63. Brettschneider J, Del Tredici K, Toledo JB, et al. Stages of pTDP-43 pathology in amyotrophic lateral sclerosis. *Ann Neurol*. 2013;74(1):20-38. doi:10.1002/ana.23937
64. Brettschneider J, Del Tredici K, Irwin DJ, et al. Sequential distribution of pTDP-43 pathology in behavioral variant frontotemporal dementia (bvFTD). *Acta Neuropathol (Berl)*. 2014;127(3):423-439. doi:10.1007/s00401-013-1238-y

## SUPPORTING INFORMATION

Additional supporting information can be found online in the Supporting Information section at the end of this article.

**How to cite this article:** Lebrun A, Leprince Y, Lagarde J, et al. How fiber bundle alterations differ in presumed LATE and amnestic Alzheimer's disease. *Alzheimer's Dement*. 2024;1-13. https://doi.org/10.1002/alz.14156